

Surface Density of Disk Galaxies in MOND

Antonino Del Popolo^{1,2} and Morgan Le Delliou^{3,4,5,*}

¹ Dipartimento di Fisica e Astronomia, University of Catania, Viale Andrea Doria 6, 95125 Catania, Italy

² Institute of Astronomy, Russian Academy of Sciences, Pyatnitskaya Str., 48, 119017 Moscow, Russia

³ Institute of Theoretical Physics, School of Physical Science and Technology, Lanzhou University, No. 222, South Tianshui Road, Lanzhou 730000, China

⁴ Instituto de Astrofísica e Ciências do Espaço, Universidade de Lisboa, Faculdade de Ciências, Ed. C8, Campo Grande, 1769-016 Lisboa, Portugal

⁵ Lanzhou Center for Theoretical Physics, Key Laboratory of Theoretical Physics of Gansu Province, Lanzhou University, Lanzhou 730000, China

* Correspondence: morgan.ledelliou.ift@gmail.com

Abstract: In this paper, we extend a paper by Milgrom (2009, MNRAS 398, 1023) dealing with the existence of a quasi-universal surface density for object of all mass and structure, if they are in the Newtonian regime, i.e., that their mean acceleration is larger than MOND typical acceleration a_0 . This result is in agreement with Donato et al. (2009)'s results, claiming the existence of a quasi-universal surface density in all masses in galaxies. The Milgrom paper also predicts that objects with mean inner acceleration smaller than the values discussed do not show the quasi-universal behavior of the surface density discussed. In the present paper, we extend the result of Milgrom's paper, based on a point mass model, considering spiral galaxies, modelled with a double exponential disk. Similar to Milgrom's results, we find the existence of a universal surface density for galaxies with large surface density, and a different behavior for galaxies having small surface density.

Keywords: galaxies; alternative theory of gravity; galaxies surface density

1. Introduction

The Λ CDM model is able to predict with high accuracy the observations on cosmological scales¹, and intermediate scales [3–8]. However, it has problems in describing the observations on small scales from tens of parsecs to some kiloparsecs. These problems are coined the so-called “small scale problems of the Λ CDM” model. One of these problems, dubbed the “Cusp/Core” problem, is the discrepancy between cuspy density profiles of galaxies in N-body simulations [9–11], and the observed cored profiles in dwarf spirals, dwarf spheroidals (dSphs), and Low Surface Brightness (LSB) galaxies [12–20]. Another problem is the “missing satellite problem” dealing with the discrepancy between the number of subhalos predicted in N-body simulations [21,22], and the one observed. A third problem is the “too-big-to-fail” problem, i.e., the subhaloes are too dense compared to what we observe around the Milky Way [23,24].

This flurry of issues remaining with the Λ CDM model has led to a debate on the validity of the dark matter (hereafter DM) assumption, as found in a Special Issue of Universe [25–34]. The debate remains vivid.

To solve the problems mentioned above, it has been proposed to modify the particles constituting DM [35–38], to modify the power spectrum (e.g., [39]), to modify the theory of gravity ([40–44], including MOND, the theory used in this work), or astrophysical solutions based on mechanisms that “heat” DM (a) supernovae feedback, and (b) transfer of energy and angular momentum from baryons to DM through dynamical friction.

In this context, using as a fitting profile a pseudo-isothermal profile, obtained through mass-modeling of the rotation curves of 55 galaxies [45], several interesting relations among the DM halos parameters were found.



Citation: Del Popolo, A.; Le Delliou, M. Surface Density of Disk Galaxies in MOND. *Universe* **2023**, *9*, 32.

<https://doi.org/10.3390/universe9010032>

Received: 23 September 2022

Revised: 23 November 2022

Accepted: 26 November 2022

Published: 1 January 2023



Copyright: © 2023 by the authors. Licensee MDPI, Basel, Switzerland. This article is an open access article distributed under the terms and conditions of the Creative Commons Attribution (CC BY) license (<https://creativecommons.org/licenses/by/4.0/>).

Among the quantities by them introduced, $\mu_{0D} = \rho_0 r_0$, is a sort of surface density, where r_0 is the core radius of the pseudo-isothermal profile, and ρ_0 its central density. In the case of late galaxies, they found that μ_{0D} was independent from galaxy luminosity, and they found a value of $\simeq 100 M_\odot / pc^2$. The previous result was extended to $\simeq 1000$ galaxies (spirals, dwarfs, ellipticals, etc.) by ([46], hereafter D09). This new work found again a quasi-universality of the central surface density of DM halos.

As already reported, Milgrom [47] used MOND, a modified gravity set at the level of Newtonian dynamics, to show that in the Newtonian regime μ_{0D} has a quasi-universal value ([48], hereafter G09). showed that the quasi-universality was present in the surface density of the luminous matter.

One issue to stress is that D09 and G09 assume that all galaxies (from dwarfs to ellipticals) have a flat inner spherical profile (note that r in this work designates the spherical radius) described by a Burkert DM halo density profile:

$$\rho(r) = \frac{\rho_0 r_0^3}{(r + r_0)(r^2 + r_0^2)}. \tag{1}$$

In reality, it is well known that the Burkert profile usually gives a good fit to the rotation curves of dwarfs and LSBs ([17,49,50], but this is not true for giant galaxies, and ellipticals, and moreover there are several exceptions [51–53]).

Since not all galaxies are fitted by a Burkert profile and have an inner flat profile, the previous discussion raises obvious doubts as to the D09 and G09 conclusions. In fact, several authors raised doubts as to the D09 and G09 results, concluding that the surface density is not universal.

For example, Napolitano et al. [54] showed that in the case of local early type galaxies the projected density within the effective radius is larger than that of dwarfs and spirals.

Ref. [55] used a much larger sample of that of D09, and G09, and showed a systematic increase with the mass of the halo. In their case, the DM column density, S , was given by

$$\log S = 0.21 \log \frac{M_{halo}}{10^{10} M_\odot} + 1.79, \tag{2}$$

with S in M_\odot / pc^2 . Cardone and Tortora [56] showed that the Newtonian acceleration and the column density correlate with different quantities: the visual luminosity L_V , the effective radius R_{eff} , the stellar mass M_* , and the halo mass M_{200} in agreement with [55], and in disagreement with the D09 and G09 results.

Napolitano et al. [54] found the non-existence of a universal surface density in early-type galaxies, while [57], in agreement with [54–56], found a correlation of the surface density with M_{200} , and [58] found a a correlation between the Newtonian acceleration and the virial mass M_{vir} . Similarly, from the analysis of Saburova et al. [59] it is clear that the DM surface density correlates with several quantities, in agreement with Zhou et al. [60] who reobtained the surface density with a Burkert profile and inferring the parameters through the Markov Chain Monte Carlo (MCMC) method.

In this paper, we extend the paper by Milgrom [47] to spiral galaxies. As in [47], objects in the Newtonian regime are characterized by a constant surface density, while objects with lower acceleration does not show this behavior. In summary, D09, and G09 conclusion that the surface density, defined as the product of the parameters ρ_0 , and r_0 of the Burkert profile, is constant for every kind of galaxies, from dwarfs to giants, is not in agreement with MOND result, apart than to all the results previously mentioned.

The paper is organized as follows. In Section 2, we discuss the methods used to obtain the parameters of DM halos which were used in the current paper and in Section 3, we discuss the results.

2. Surface Density

Mass and mass densities may be measured by means of their gravitational effects on the trajectories of massive particles. In the following we follow [47,61].

If the acceleration field is given by $\mathbf{g}(\mathbf{r})$, this can be obtained from the potential ϕ : $\mathbf{g}(\mathbf{r}) = -\nabla \phi$ which gives rise to the Poisson equation $\nabla^2 \phi = 4\pi G \rho^*$. The gravitational mass density $\rho^*(\mathbf{r})$ is given by

$$\rho^*(\mathbf{r}) = \frac{1}{4\pi G} \nabla \cdot \mathbf{g}(\mathbf{r}). \tag{3}$$

In case the Newtonian dynamics are not applicable the quantity $\rho^*(\mathbf{r})$ is not the true density $\rho(\mathbf{r})$ giving rise to $\mathbf{g}(\mathbf{r})$. One then defines the phantom mass density given by $\rho_P(\mathbf{r}) = \rho^*(\mathbf{r}) - \rho(\mathbf{r})$. The phantom density ρ_P is considered as a real quantity but not observed to date.

The quantity $\rho(\mathbf{r})$ is given by

$$\rho(\mathbf{r}) = -\frac{1}{4\pi G} \nabla \cdot [\mu(g/a_0) \mathbf{g}]. \tag{4}$$

Ref. [61], where $\mu(x)$ is the interpolating function, and a_0 is the MOND acceleration constant. Equation (4) does not fix $\mathbf{g}(\mathbf{r})$ uniquely for a given $\rho(\mathbf{r})$. \mathbf{g} is determined uniquely if in addition to Equation (4) we require $\mathbf{g} = -\nabla \phi$. Equation (4) can be written doing the derivatives

$$\begin{aligned} \rho &= \frac{-1}{4\pi G} \{ \nabla \cdot \mathbf{g}[\mu(g/a_0)] + \mathbf{g} \cdot \nabla [\mu(g/a_0)] \} = \\ &\rho^* \mu(g/a_0) - \frac{1}{4\pi G} \mu'(g/a_0) a_0^{-1} \mathbf{g} \cdot \nabla \mathbf{g}. \end{aligned} \tag{5}$$

We then may write

$$\begin{aligned} \rho_P(\mathbf{r}) &= \rho^* - \rho = \rho^* - \rho^* \mu + \frac{1}{4\pi G} \frac{\mu'}{a_0} \mathbf{g} \cdot \nabla \mathbf{g} = \\ &\rho^*(1 - \mu) + \frac{1}{4\pi G} L \mu \mathbf{e}_g \cdot \nabla \mathbf{g}, \end{aligned} \tag{6}$$

where $L = \frac{\mu'}{\mu} g/a_0$. Recalling that $\rho^* = \rho + \rho_P$, we have

$$\rho_P = (\rho + \rho_P)(1 - \mu) + \frac{1}{4\pi G} L \mu \mathbf{e}_g \cdot \nabla \mathbf{g}, \tag{7}$$

and simplifying

$$\rho_P(\mathbf{r}) = \rho(\mathbf{r}) \left(\frac{1}{\mu} - 1 \right) + \frac{1}{4\pi G} L \mu \mathbf{e}_g \cdot \nabla \mathbf{g}. \tag{8}$$

This last equation can be written in terms of the potential recalling that $\mathbf{g} = -\nabla \phi$:

$$\rho_P(\mathbf{r}) = -\frac{1}{4\pi G a_0} \frac{\mu'}{\mu} \nabla |\nabla \phi| \nabla \phi + \rho(\mathbf{r}) (1/\mu - 1). \tag{9}$$

Defining $\mathcal{V}(x) = \int L(x) dx$, with $x = g/a_0$, $L = \frac{\mu'}{\mu} x$, and defining a vector \mathbf{e} in the direction of $\nabla \phi$, we can write

$$\rho_P = \rho_{P_1} + \rho_{P_2} = \frac{-a_0}{4\pi G} \mathbf{e} \cdot \nabla \mathcal{V} (|\nabla \phi|/a_0) + (1/\mu - 1) \rho, \tag{10}$$

and

$$\rho_{P_1} = \frac{-a_0}{4\pi G} \mathbf{e} \nabla \mathcal{V} (|\nabla \phi|/a_0), \tag{11}$$

$$\rho_{P_2} = (1/\mu - 1)\rho. \tag{12}$$

In the case of a point mass, the central surface density given by Equation (11) can be obtained integrating ρ_P as

$$\begin{aligned} \Sigma(0) &= \int_{-\infty}^{+\infty} (\rho_{P_1} + \rho_{P_2})dz = 2 \int_0^{\infty} (\rho_{P_1} + (1/\mu - 1)\rho)dz = \\ &= \Sigma_M[\mathcal{V}(\infty) - \mathcal{V}(0)] + 0 = \\ &= \Sigma_M \int_0^{\infty} L(x)dx = a\Sigma_M, \end{aligned} \tag{13}$$

where $\Sigma_M = \frac{a_0}{2\pi G}$. Please note that the integral of ρ_{P_2} is zero because inside the mass $\mu \simeq 1$. The value of a depends on the interpolation function. For example, for $n = 2$, $\mu = \frac{x}{(1+x^2)^{1/2}}$, we have $\frac{\pi}{2}\Sigma_M$ and for larger n the value of a tends to 1.

D09 gives a surface density integrating the Burkert profile², given by

$$\Sigma_0 = 2 \int \rho dr = 2 \int \frac{\rho_0 r_0^3}{(r + r_0)(r^2 + r_0^2)} = \frac{\pi}{2} \rho_0 r_0 = \frac{\pi}{2} \Sigma_c. \tag{14}$$

If we call Σ_c^* the MOND analog of Σ_c we have, using the MOND to non-MOND surface density ratio λ introduced in [47],

$$\Sigma_c^* = \frac{2\lambda}{\pi} \Sigma_M, \tag{15}$$

with $\Sigma_M = 138 \frac{a_0}{1.2 \times 10^{-8} \text{cms}^{-2}} M_{\odot} / pc^2$.

Our main goal is to extend the previous point mass calculation to the case of disk systems. As we saw, Equation (11) may be applied to spherical systems, but it can also be applied to disk systems.

To calculate the integral of Equation (10) we will distinguish two cases, the one in which $x \geq 1$ (acceleration above the MOND universal constant), and the other in which $x \leq 1$. At this stage it is worth pointing out that in our theoretical study we focus on galaxies which are clearly in the $x \gg 1$ or $x \ll 1$ regimes. Since any qualitative behavior in the intermediate regime will smoothly connect the two, we are not interested in the quantitative details of such regime and will imply the clear regimes when referring to either $x \geq 1$ or $x \leq 1$ in what follows. Let us consider the second term (Equation (12)), $\rho_{P_2} = (1/\mu - 1)\rho$.

The dimensionless acceleration, obtained from the ratio of the Newtonian acceleration $(\mu(g/a_0)g)$ and a_0 , is given by $a_N = (g/a_0)\mu(g/a_0)$. If we use $n = 1$, and $\mu = \frac{x}{(1+x^2)^{1/2}} = \frac{g/a_0}{1+g/a_0}$, multiplying for μ we have

$$\mu = \frac{\mu g/a_0}{\mu g/a_0 + \mu} = \frac{a_N}{a_N + \mu}, \tag{16}$$

solving with respect to μ we have

$$\mu = -1/2a_N + 1/2\sqrt{a_N^2 + 4a_N}. \tag{17}$$

Here we used $n = 1$ to have an algebraically simplified form of the acceleration. Using $n = 2$ complicates the algebra but the following results do not change.

For a double exponential disk, with cylindrical radius R and altitude z ,

$$\rho = \rho_0 e^{-R/h_r - |z|/h_z}, \tag{18}$$

the surface density is

$$\Sigma = \int_0^{\infty} \rho dz, \tag{19}$$

and the mass

$$M = \int_0^\infty 2\pi R \Sigma dz = 2\pi \rho_0 h_z h_r^2, \tag{20}$$

while the dimensionless MOND acceleration ratio, in a similar way as in [47], reads (with Σ_b , the baryonic surface density, approximated by an integrated constant volume density $\Sigma_b \simeq \int \rho_0 dz = \rho_0 h_z$)

$$a_N \simeq \frac{GM}{a_0 R^2} = \frac{G2\pi\rho_0 h_z h_r^2}{a_0 R^2} \simeq \frac{\Sigma_b}{\Sigma_M} \frac{h_r^2}{R^2}. \tag{21}$$

The acceleration here is approximated using the spherical expression in cylindrical symmetry. Such an approximation can be evaluated using, for instance, ([62], Equation 2.165) to compare with the spherical expression and obtain an error within some percent in the inner disk and within 10% in the outer disk. The MOND interpolating function becomes

$$\mu = -1/2 \frac{\Sigma_b h_r^2}{\Sigma_M R^2} + 1/2 \sqrt{\frac{\Sigma_b^2 h_r^4}{\Sigma_M^2 R^4} + 4 \frac{\Sigma_b h_r^2}{\Sigma_M R^2}}. \tag{22}$$

Please note that the MOND acceleration being defined as a radial acceleration following [47], the gravitational potential is approximated with the spherical expression. Since in the inner parts of the system, the error of the approximation with respect to a thin disk is of the order of some percent and some 10 percent further away where MOND is valid, and we are evaluating qualitative behaviors, we only introduce the cylindrical disk geometry at the level of the mass distribution. Then

$$\begin{aligned} \frac{1-\mu}{\mu} \int_{-\infty}^{+\infty} \rho dz &\simeq \frac{2(1-\mu)}{\mu} \Sigma_b \exp^{-R/h_r} \\ &= \frac{2(1-\mu)}{\mu} a_N \Sigma_M \frac{R^2}{h_r^2} \exp^{-R/h_r} \\ &= \frac{2(1-\mu)}{\mu} x \mu \Sigma_M \frac{R^2}{h_r^2} \exp^{-R/h_r} \\ &= 2(1-\mu) x \Sigma_M \frac{R^2}{h_r^2} \exp^{-R/h_r}. \end{aligned} \tag{23}$$

The full integral can be written as

$$F = F_1 + F_2 = \frac{2}{\pi} \Sigma_M \int_0^x L(x) dx + \frac{2}{\pi} 2(1-\mu) x \Sigma_M \frac{R^2}{h_r^2} \exp^{-R/h_r}. \tag{24}$$

CASE $x \leq 1$

We recall that $g = a_0 x$, and in the case $x \leq 1$, $\mu = x$, $a_N = (g/a_0)\mu = x^2$, and from $a_N = x^2 = \frac{\Sigma_b}{\Sigma_M} \frac{h_r^2}{R^2}$, $x = \sqrt{\frac{\Sigma_b}{\Sigma_M} \frac{h_r}{R}}$.

Concerning the first term F_1 ,

$$F_1 = \frac{2}{\pi} \Sigma_M \int_0^x L(x) dx, \tag{25}$$

using $\mu = x/\sqrt{1+x^2}$, recalling that $L = \frac{\mu'}{\mu} x$, and $x = \sqrt{\frac{\Sigma_b}{\Sigma_M} \frac{h_r}{R}}$, one can obtain F_1 in terms of $\frac{\Sigma_b}{\Sigma_M}$, and for small x or small $\frac{\Sigma_b}{\Sigma_M}$ we obtain

$$\begin{aligned} F_1 &= \frac{2}{\pi} \Sigma_M \int_0^x L(x) dx = \frac{2}{\pi} \Sigma_M \arctan x \\ &= \frac{2}{\pi} \Sigma_M \arctan \left(\sqrt{\frac{\Sigma_b}{\Sigma_M} \frac{h_r}{R}} \right). \end{aligned} \tag{26}$$

Substituting Equation (22) in the right term F_2 of Equation (24) we obtain

$$F_2 = \frac{2}{\pi} 2 \frac{R \Sigma_M}{h_r} \left(1 + 1/2 \frac{\Sigma_b h_r^2}{\Sigma_M R^2} - 1/2 \sqrt{\frac{\Sigma_b^2 h_r^4}{\Sigma_M^2 R^4} + 4 \frac{\Sigma_b h_r^2}{\Sigma_M R^2}} \right) \times \sqrt{\frac{\Sigma_b}{\Sigma_M}} e^{-\frac{R}{h_r}}, \tag{27}$$

that at first order can be written as

$$F_2 = (4/\pi) \frac{h_r \Sigma_M}{R} e^{-\frac{R}{h_r}} \sqrt{\frac{\Sigma_b}{\Sigma_M}}. \tag{28}$$

Then we have that

$$F = \frac{2}{\pi} \Sigma_M \arctan \left(\sqrt{\frac{\Sigma_b}{\Sigma_M}} \frac{h_r}{R} \right) + \frac{2}{\pi} 2 \frac{R \Sigma_M}{h_r} \left(1 + 1/2 \frac{\Sigma_b h_r^2}{\Sigma_M R^2} - 1/2 \sqrt{\frac{\Sigma_b^2 h_r^4}{\Sigma_M^2 R^4} + 4 \frac{\Sigma_b h_r^2}{\Sigma_M R^2}} \right) \times \sqrt{\frac{\Sigma_b}{\Sigma_M}} e^{-\frac{R}{h_r}}. \tag{29}$$

At small x F_1 tend to zero, and F is dominated by the second term.

CASE $x \geq 1$

Concerning the case $x \geq 1$, we have again Equation (24)

$$F = \frac{2}{\pi} \Sigma_M \int_0^x L(x) dx + (4/\pi) (1 - \mu) x \Sigma_M \frac{R^2}{h_r^2} \exp^{-R/h_r}. \tag{30}$$

Recalling that $L = \frac{\mu'}{\mu} x$, $x = \frac{\Sigma_b}{\Sigma_M} \frac{h_r^2}{R^2}$ for $\mu = \frac{x}{\sqrt{1+x^2}}$ we have

$$F_1 = \frac{2}{\pi} \Sigma_M \int_0^x L(x) dx = \frac{2}{\pi} \Sigma_M \arctan x = \frac{2}{\pi} \Sigma_M \arctan \left(\frac{\Sigma_b}{\Sigma_M} \frac{h_r^2}{R^2} \right), \tag{31}$$

and

$$F_2 = \frac{4}{\pi} \left(1 + 1/2 \frac{\Sigma_b h_r^2}{\Sigma_M R^2} - 1/2 \sqrt{\frac{\Sigma_b^2 h_r^4}{\Sigma_M^2 R^4} + 4 \frac{\Sigma_b h_r^2}{\Sigma_M R^2}} \right) \times x \Sigma_M e^{-\frac{R}{h_r}} R^2 / h_r^2, \tag{32}$$

so for $x \geq 1$, or $\Sigma_b \geq \Sigma_M$, $x = \frac{\Sigma_b}{\Sigma_M} \frac{h_r^2}{R^2}$, we have

$$\begin{aligned}
 F &= \frac{2}{\pi} \Sigma_M \arctan \left(\frac{\Sigma_b h_r^2}{\Sigma_M R^2} \right) + \\
 &\frac{4}{\pi} \left(1 + 1/2 \frac{\Sigma_b h_r^2}{\Sigma_M R^2} - 1/2 \sqrt{\frac{\Sigma_b^2 h_r^4}{\Sigma_M^2 R^4} + 4 \frac{\Sigma_b h_r^2}{\Sigma_M R^2}} \right) \\
 &\times \Sigma_M e^{-\frac{R}{h_r} R^2/h_r^2}.
 \end{aligned}
 \tag{33}$$

For large x , F_2 tends to 0, $O(1)$, and $F_1 \simeq \Sigma_M$.

Assuming $h_r = R$, which corresponds to focusing at the edge of the central region of the galaxy where measurement of the central surface density is clearer, we plot in the left panel of Figure 1 the Σ_c^* in terms of Σ_b/Σ_M , representing the 1σ errors of the evaluation, propagated from the spherical potential approximation, with shaded areas bounded by dashed curves.

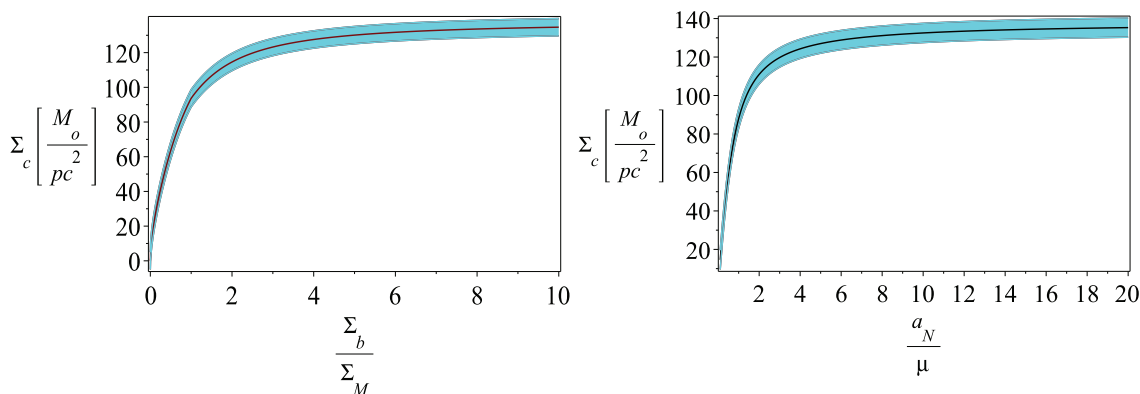


Figure 1. Left panel: the MOND column density in terms of the ratio Σ_b/Σ_M . Right panel: The MOND column density in terms of the ratio of the acceleration, a_N , and μ . In both panels, the shaded regions bounded by dashed curves represent the 1σ evaluation induced by the approximations described in the text.

The figure shows that there is a double trend of the surface density. At small Σ_b/Σ_M , for $R = h_r$, the surface density increases as $\sqrt{\frac{\Sigma_b}{\Sigma_M}} \Sigma_M$. Going to larger Σ_b/Σ_M , the plot flattens till when, at large Σ_b/Σ_M tends to Σ_M . The previous results, plotted in the left panel of Figure 1, rely on assuming that the behavior at intermediate values of x and Σ_b/Σ_M should remain smooth. This is vindicated by the exact calculation below, leading to Equation (34) and the plotting of Figure 1’s right panel, and which is independent of the previous approximations.

Apart the dependence of Σ_c^* on the ratio Σ_b/Σ_M , the dependence from the acceleration a_N/μ can be obtained by the relation

$$\begin{aligned}
 F &= \frac{2}{\pi} \Sigma_M \int_0^x L(x) dx + \frac{4}{\pi} (1 - \mu) x \Sigma_M \frac{R^2}{h_r^2} \exp^{-R/h_r} \\
 &= \frac{2}{\pi} \Sigma_M \arctan x + \frac{4}{\pi} (1 - \mu) x \Sigma_M \frac{R^2}{h_r^2} \exp^{-R/h_r},
 \end{aligned}
 \tag{34}$$

with the previous definition of $\mu = \frac{x}{\sqrt{1+x^2}}$, and $L(x) = x \frac{\mu'}{\mu}$, and assuming $h_r = R$, we plot in the right panel of Figure 1 the relation Σ_c^* versus a_N/μ .

As in the left panel of Figure 1, the plot shows again a double trend of the surface density. At small $x = g/a_0$, for $R = h_r$, the surface density increases as $x \Sigma_M$. Going to larger x , the plot flattens and reach the asymptote Σ_M . The behavior in the right panel of Figure 1 deriving from Equation (34), it is exact. As the left panel displays a similar

asymptotic behavior to the right panel for both $a_N \ll a_0$ and $a_N \gg a_0$, and we expect a smooth junction between the two regions, the plotting of the smooth junction is justified.

The previous plots and the result of the present paper can be summarized as follows, and represent the main result of the paper. The previous results show that the claim of existence of a quasi-universal surface density in agreement with D09, and G09, is in disagreement with MOND, which predicts that for small values of baryonic surface density Σ_b , or small acceleration, the surface density decreases below the quasi-universal value. This result is also in agreement with [54–60], namely the surface density is not universal. The D09 and G09 claims of the existence of a quasi-universal value of the surface density for all galaxies (considering low surface density ones) is denied also from the existence of galaxies having values much smaller than Σ_M . As an example, NGC 3741 according to [63] has a value $56M_\odot/pc^2$ much smaller than the quasi-universal value, or similarly KK98 250, KK98 251 has shown by [64] have values $56M_\odot/pc^2$, and $66M_\odot/pc^2$. In a future paper, we want to use the SPARC sample to determine the values of the surface density and compare with our model. One question that could arise, is why does D09 claim the universality of the surface density? Probably this is due to the fact they had few galaxies at small surface density, and they were plagued by errors. In their Figure 2, from magnitude -15 to 7 , they had just seven galaxies. One is NGC 2137, whose surface density errors were probably overestimated. The others are dwarf spheroidals, that as reported by the same D09 is beset with uncertainties in the model assumptions, leading to non-unique results. Concerning high surface density systems, the D09 result is in agreement with MOND, namely there is a quasi-universal surface density.

The MOND prediction of the non-existence of a universal surface density on a large range of surface densities or acceleration, is in agreement with several studies [54–60], which disagrees with D09 result.

3. Discussion

We extended a paper of Milgrom related to the prediction of the existence of a quasi-universal central density surface density of dark halos. According to this study, systems characterized by a mean acceleration larger than MOND typical acceleration a_0 , namely if they are in Newtonian regime, are characterized by a quasi-universal surface density, whose value is proportional to $\Sigma_M = \frac{a_0}{2\pi G} = 138 \frac{a_0}{1.2 \times 10^{-8} \text{cms}^{-2}} M_\odot/pc^{-2}$. This claim is in agreement with those of D09 and G09. Milgrom [47] also calculated in the case of general (non-disky) systems with constant density, an approximated value for the surface density, showing that for systems of low surface density there is no longer a quasi-universal value, but the studied systems are characterized by lower values of the surface density, which contradicts D09. In the present paper, the calculation of Milgrom, set from a point mass model, was extended to spiral galaxies, modeled with a cylindrically symmetric double exponential disk. We found a quasi-universal surface density for Newtonian systems, and confirmed smaller values of the surface density for low acceleration systems in our extended cylindrical configuration.

Author Contributions: All authors have contributed equally in this work. All authors have read and agreed to the published version of the manuscript.

Funding: MLeD acknowledges financial support by the Lanzhou University starting fund, the Fundamental Research Funds for the Central Universities (Grant No. lzujbky-2019-25), the National Science Foundation of China (grant No. 12047501), and the 111 Project under Grant No. B20063.

Institutional Review Board Statement: Not applicable.

Informed Consent Statement: Not applicable.

Data Availability Statement: Not applicable.

Acknowledgments: The authors wish to thank Francesco Pace for some calculations.

Conflicts of Interest: The authors declare no conflict of interest.

Notes

- ¹ we recall that at cosmological scales the Λ CDM paradigm is affected by the cosmological constant problem [1,2].
- ² Please note that since the profile is spherically symmetric, integrating along an axis direction z is equivalent to integrating twice along the positive radial direction

References

1. Weinberg, S. The cosmological constant problem. *Rev. Mod. Phys.* **1989**, *61*, 1–23. [[CrossRef](#)]
2. Astashenok, A.V.; Popolo, A. Cosmological measure with volume averaging and the vacuum energy problem. *Class. Quantum Gravity* **2012**, *29*, 085014. [[CrossRef](#)]
3. Spergel, D.N.; Verde, L.; Peiris, H.V.; Komatsu, E.; Nolta, M.R.; Bennett, C.L.; Halpern, M.; Hinshaw, G.; Jarosik, N.; Kogut, A.; et al. First-Year Wilkinson Microwave Anisotropy Probe (WMAP) Observations: Determination of Cosmological Parameters. *Astrophys. J. Suppl. Ser.* **2003**, *148*, 175–194. [[CrossRef](#)]
4. Kowalski, M.; Rubin, D.; Aldering, G.; Agostinho, R.J.; Amadon, A.; Amanullah, R.; Balland, C.; Barbary, K.; Blanc, G.; Challis, P.J.; et al. Improved Cosmological Constraints from New, Old, and Combined Supernova Data Sets. *Astrophys. J.* **2008**, *686*, 749–778. [[CrossRef](#)]
5. Percival, W.J.; Reid, B.A.; Eisenstein, D.J.; Bahcall, N.A.; Budavari, T.; Frieman, J.A.; Fukugita, M.; Gunn, J.E.; Ivezić, E.A. Baryon acoustic oscillations in the Sloan Digital Sky Survey Data Release 7 galaxy sample. *Mon. Not. R. Astron. Soc.* **2010**, *401*, 2148–2168. [[CrossRef](#)]
6. Komatsu, E.; Smith, K.M.; Dunkley, J.; Bennett, C.L.; Gold, B.; Hinshaw, G.; Jarosik, N.; Larson, D.; Nolta, M.R.; Page, L.E.A. Seven-year Wilkinson Microwave Anisotropy Probe (WMAP) Observations: Cosmological Interpretation. *Astrophys. J. Suppl. Ser.* **2011**, *192*, 18. [[CrossRef](#)]
7. Popolo, A. Non-baryonic dark matter in cosmology. *Am. Inst. Phys.* **2013**, *1548*, 2–63. [[CrossRef](#)]
8. Popolo, A. Nonbaryonic Dark Matter in Cosmology. *Int. J. Mod. Phys. D* **2014**, *23*, 30005. [[CrossRef](#)]
9. Navarro, J.F.; Frenk, C.S.; White, S.D.M. The Structure of Cold Dark Matter Halos. *Astrophys. J.* **1996**, *462*, 563. [[CrossRef](#)]
10. Navarro, J.F.; Frenk, C.S.; White, S.D.M. A Universal Density Profile from Hierarchical Clustering. *Astrophys. J.* **1997**, *490*, 493. [[CrossRef](#)]
11. Navarro, J.F.; Ludlow, A.; Springel, V.; Wang, J.; Vogelsberger, M.; White, S.D.M.; Jenkins, A.; Frenk, C.S.; Helmi, A. The diversity and similarity of simulated cold dark matter haloes. *Mon. Not. R. Astron. Soc.* **2010**, *402*, 21–34. [[CrossRef](#)]
12. Moore, B. Evidence against dissipation-less dark matter from observations of galaxy haloes. *Nature* **1994**, *370*, 629–631. [[CrossRef](#)]
13. Flores, R.A.; Primack, J.R. Observational and theoretical constraints on singular dark matter halos. *arXiv* **1994**, *427*, L1–L4. [[CrossRef](#)]
14. Burkert, A. The Structure of Dark Matter Halos in Dwarf Galaxies. *Astrophys. J.* **1995**, *447*, L25. [[CrossRef](#)]
15. Blok, W.J.G.; Bosma, A.; McGaugh, S. Simulating observations of dark matter dominated galaxies: Towards the optimal halo profile. *Mon. Not. R. Astron. Soc.* **2003**, *340*, 657–678. [[CrossRef](#)]
16. Swaters, R.A.; Madore, B.F.; den Bosch, F.C.; Balcells, M. The Central Mass Distribution in Dwarf and Low Surface Brightness Galaxies. *Astrophys. J.* **2003**, *583*, 732–751. [[CrossRef](#)]
17. Popolo, A. The Cusp/Core Problem and the Secondary Infall Model. *Astrophys. J.* **2009**, *698*, 2093–2113. [[CrossRef](#)]
18. Popolo, A.; Kroupa, P. Density profiles of dark matter haloes on galactic and cluster scales. *Astron. Astrophys.* **2009**, *502*, 733–747. [[CrossRef](#)]
19. Popolo, A. Density profile slopes of dwarf galaxies and their environment. *Mon. Not. R. Astron. Soc.* **2012**, *419*, 971–984. [[CrossRef](#)]
20. Popolo, A.; Hiottel, N. Cusps and cores in the presence of galactic bulges. *J. Cosmol. Astropart. Phys.* **2014**, *1*, 47. [[CrossRef](#)]
21. Klypin, A.; Kravtsov, A.V.; Valenzuela, O.; Prada, F. Where Are the Missing Galactic Satellites? *Astrophys. J.* **1999**, *522*, 82–92. [[CrossRef](#)]
22. Moore, B.; Quinn, T.; Governato, F.; Stadel, J.; Lake, G. Cold collapse and the core catastrophe. *Mon. Not. R. Astron. Soc.* **1999**, *310*, 1147–1152. [[CrossRef](#)]
23. Garrison-Kimmel, S.; Rocha, M.; Boylan-Kolchin, M.; Bullock, J.S.; Lally, J. Can feedback solve the too-big-to-fail problem? *Mon. Not. R. Astron. Soc.* **2013**, *433*, 3539–3546. [[CrossRef](#)]
24. Garrison-Kimmel, S.; Boylan-Kolchin, M.; Bullock, J.S.; Kirby, E.N. Too big to fail in the Local Group. *Mon. Not. R. Astron. Soc.* **2014**, *444*, 222–236. [[CrossRef](#)]
25. Feng, J.Q. Rotating disk galaxies without dark matter based on scientific reasoning. *Galaxies* **2020**, *8*, 9. [[CrossRef](#)]
26. Marr, J.H. Entropy and mass distribution in disc galaxies. *Galaxies* **2020**, *8*, 12. [[CrossRef](#)]
27. Criss, R.E.; Hofmeister, A.M. Density profiles of 51 galaxies from parameter-free inverse models of their measured rotation curves. *Galaxies* **2020**, *8*, 19. [[CrossRef](#)]
28. McGaugh, S. Predictions and outcomes for the dynamics of rotating galaxies. *Galaxies* **2020**, *8*, 35. [[CrossRef](#)]
29. Sipols, A.; Pavlovich, A. Dark matter dogma: A study of 214 galaxies. *Galaxies* **2020**, *8*, 36. [[CrossRef](#)]
30. Sofue, Y. Rotation curve of the milky way and the dark matter density. *Galaxies* **2020**, *8*, 37. [[CrossRef](#)]
31. Sofue, Y. Gravitational focusing of low-velocity dark matter on the earth's surface. *Galaxies* **2020**, *8*, 42. [[CrossRef](#)]

32. Hofmeister, A.M.; Criss, R.E. Debated models for galactic rotation curves: A review and mathematical assessment. *Galaxies* **2020**, *8*, 47. [[CrossRef](#)]
33. Sipols, A.; Pavlovich, A. Surface brightness plateau in s4g galaxies. *Galaxies* **2020**, *8*, 48. [[CrossRef](#)]
34. Hofmeister, A.M.; Criss, R.E. Debate on the physics of galactic rotation and the existence of dark matter. *Galaxies* **2020**, *8*, 54. [[CrossRef](#)]
35. Colín, P.; Avila-Reese, V.; Valenzuela, O. Substructure and Halo Density Profiles in a Warm Dark Matter Cosmology. *Astrophys. J.* **2000**, *542*, 622–630. [[CrossRef](#)]
36. Sommer-Larsen, J.; Dolgov, A. Formation of Disk Galaxies: Warm Dark Matter and the Angular Momentum Problem. *Astrophys. J.* **2001**, *551*, 608–623. [[CrossRef](#)]
37. Goodman, J. Repulsive dark matter. *New Astron.* **2000**, *5*, 103–107. [[CrossRef](#)]
38. Peebles, P.J.E. Fluid Dark Matter. *Astrophys. J.* **2000**, *534*, L127–L129. [[CrossRef](#)]
39. Zentner, A.R.; Bullock, J.S. Halo Substructure and the Power Spectrum. *Astrophys. J.* **2003**, *598*, 49–72. [[CrossRef](#)]
40. Buchdahl, H.A. Non-linear Lagrangians and cosmological theory. *Mon. Not. R. Astron. Soc.* **1970**, *150*, 1. [[CrossRef](#)]
41. Starobinsky, A.A. A new type of isotropic cosmological models without singularity. *Phys. Lett. B* **1980**, *91*, 99–102. [[CrossRef](#)]
42. Milgrom, M. A modification of the Newtonian dynamics as a possible alternative to the hidden mass hypothesis. *Astrophys. J.* **1983**, *270*, 365–370. [[CrossRef](#)]
43. Milgrom, M. A modification of the Newtonian dynamics—Implications for galaxies. *Astrophys. J.* **1983**, *270*, 371–389. [[CrossRef](#)]
44. Ferraro, R. $f(R)$ and $f(T)$ theories of modified gravity. *AIP Conf. Proc.* **2012**, *1471*, 103–110. [[CrossRef](#)]
45. Kormendy, J.; Freeman, K.C. Scaling Laws for Dark Matter Halos in Late-Type and Dwarf Spheroidal Galaxies. *arXiv* **2004**, *220*, 377. [[CrossRef](#)]
46. Donato, F.; Gentile, G.; Salucci, P.; Martins, C.; Wilkinson, M.I.; Gilmore, G.; Grebel, E.K.; Koch, A.; Wyse, R. A constant dark matter halo surface density in galaxies. *Mon. Not. R. Astron. Soc.* **2009**, *397*, 1169–1176. [[CrossRef](#)]
47. Milgrom, M. The central surface density of ‘dark haloes’ predicted by MOND. *Mon. Not. R. Astron. Soc.* **2009**, *398*, 1023–1026. [[CrossRef](#)]
48. Gentile, G.; Famaey, B.; Zhao, H.; Salucci, P. Universality of galactic surface densities within one dark halo scale-length. *Nature* **2009**, *461*, 627–628. [[CrossRef](#)]
49. Gentile, G.; Salucci, P.; Klein, U.; Vergani, D.; Kalberla, P. The cored distribution of dark matter in spiral galaxies. *Mon. Not. R. Astron. Soc.* **2004**, *351*, 903–922. [[CrossRef](#)]
50. Gentile, G.; Salucci, P.; Klein, U.; Granato, G.L. NGC 3741: The dark halo profile from the most extended rotation curve. *Mon. Not. R. Astron. Soc.* **2007**, *375*, 199–212. [[CrossRef](#)]
51. Simon, J.D.; Bolatto, A.D.; Leroy, A.; Blitz, L.; Gates, E.L. High-Resolution Measurements of the Halos of Four Dark Matter-Dominated Galaxies: Deviations from a Universal Density Profile. *Astrophys. J.* **2005**, *621*, 757–776. [[CrossRef](#)]
52. Blok, W.J.G.; Walter, F.; Brinks, E.; Trachternach, C.; Oh, S.-H.; Kennicutt, R.C., Jr. High-Resolution Rotation Curves and Galaxy Mass Models from THINGS. *Astron. J.* **2008**, *136*, 2648–2719. [[CrossRef](#)]
53. Popolo, A. On the density-profile slope of clusters of galaxies. *Mon. Not. R. Astron. Soc.* **2012**, *424*, 38–51. [[CrossRef](#)]
54. Napolitano, N.R.; Romanowsky, A.J.; Tortora, C. The central dark matter content of early-type galaxies: Scaling relations and connections with star formation histories. *Mon. Not. R. Astron. Soc.* **2010**, *405*, 2351–2371. [[CrossRef](#)]
55. Boyarsky, A.; Ruchayskiy, O.; Iakubovskiy, D.; Maccio’, A.V.; Malyshev, D. New evidence for dark matter. *arXiv* **2009**, arXiv:0911.1774.
56. Cardone, V.F.; Tortora, C. Dark matter scaling relations in intermediate z haloes. *Mon. Not. R. Astron. Soc.* **2010**, *409*, 1570–1576. [[CrossRef](#)]
57. Popolo, A.; Cardone, V.F.; Belvedere, G. Surface density of dark matter haloes on galactic and cluster scales. *Mon. Not. R. Astron. Soc.* **2013**, *429*, 1080–1087. [[CrossRef](#)]
58. Cardone, V.F.; Popolo, A. Newtonian acceleration scales in spiral galaxies. *Mon. Not. R. Astron. Soc.* **2012**, *427*, 3176–3187. [[CrossRef](#)]
59. Saburova, A.; Popolo, A. On the surface density of dark matter haloes. *Mon. Not. R. Astron. Soc.* **2014**, *445*, 3512–3524. [[CrossRef](#)]
60. Zhou, Y.; Popolo, A.; Chang, Z. On the absence of a universal surface density, and a maximum Newtonian acceleration in dark matter haloes: Consequences for MOND. *Phys. Dark Universe* **2020**, *28*, 100468. [[CrossRef](#)]
61. Milgrom, M. Can the Hidden Mass Be Negative? *Astrophys. J.* **1986**, *306*, 9. [[CrossRef](#)]
62. Binney, J.; Tremaine, S. *Galactic Dynamics*, 2nd ed.; Princeton University Press: Princeton, NJ, USA, 2008.
63. Begum, A.; Chengalur, J.N.; Karachentsev, I.D. A dwarf galaxy with a giant HI disk. *Astron. Astrophys.* **2005**, *433*, L1–L4. [[CrossRef](#)]
64. Begum, A.; Chengalur, J.N. Kinematics of two dwarf galaxies in the NGC 6946 group. *Astron. Astrophys.* **2004**, *424*, 509–517. [[CrossRef](#)]

Disclaimer/Publisher’s Note: The statements, opinions and data contained in all publications are solely those of the individual author(s) and contributor(s) and not of MDPI and/or the editor(s). MDPI and/or the editor(s) disclaim responsibility for any injury to people or property resulting from any ideas, methods, instructions or products referred to in the content.